

## Electronic Supplementary Information

### Properties of sonochemically functionalized nonsteroidal anti-inflammatory drug ketorolac in Fe<sub>3</sub>O<sub>4</sub>-graphene oxide nanocomposite

Vladimir Fedosenko,<sup>a</sup> Anna Matsukovich,<sup>b</sup> Ludmila Tabulina,<sup>a</sup> Vladimir Labunov<sup>a</sup> and Darya Radziuk<sup>\*a</sup>

Content:

- 1) Experimental section;
- 2) Characterization;
- 3) Detailed analysis of synthesized graphene oxide (GO) powder in the use of XRD pattern, Raman and FT-IR spectra, and EDX analysis;
- 4) DLS diagrams and ZP curves of GO, Fe<sub>3</sub>O<sub>4</sub> nanoparticles and Fe<sub>3</sub>O<sub>4</sub>-GO nanocomposite;
- 5) Detailed XRD analysis of Fe<sub>3</sub>O<sub>4</sub>-GO nanocomposite and its EDX spectrum;
- 6) Detailed XRD analysis of preformed Fe<sub>3</sub>O<sub>4</sub> nanoparticles;
- 7) Modelled chemical structure of ketorolac;
- 8) Control experiments: UV-Vis absorbance spectra of pristine ketorolac, ketorolac-Fe<sub>3</sub>O<sub>4</sub> and ketorolac-GO in aqueous solutions at pH = 1, 5 or 8 after 7 h of incubation;
- 9) List of references.

## Experimental Section

### *Materials*

Graphite was purchased from IMERYYS, France (detailed information about the graphite size and elemental composition can be found in reference<sup>[1]</sup>).  $\text{H}_3\text{PO}_4$ ,  $\text{KMnO}_4$ ,  $\text{H}_2\text{SO}_4$ ,  $\text{H}_2\text{O}_2$  (60%),  $\text{HCl}$  (35%),  $\text{HNO}_3$  (40%),  $\text{C}_2\text{H}_5\text{OH}$ ,  $\text{C}_3\text{H}_8\text{O}$ ,  $\text{FeCl}_3 \cdot 6 \text{H}_2\text{O}$ ,  $\text{FeCl}_2 \cdot 4 \text{H}_2\text{O}$  are of higher grade purity 99% being obtained from Belreachim JSC (The Republic of Belarus). Distilled water (pH = 5.5, specific conductivity 5  $\mu\text{S}/\text{cm}$ ) was prepared by using a homemade distillation apparatus (The Republic of Belarus). Ketorolac was purchased from Dr. Reddy's Inc. (India). For experiments 10 tablets of ketorolac were grinded in a mortar until a fine powder was obtained. This powder was dissolved in 3 mL of ethanol at a critical concentration of drug dissolution being 7 g/L.

### *Synthesis of graphene oxide (GO)*

Graphene oxide (GO) was synthesized by using the improved Hummers method<sup>[2]</sup> and more details can be found in reference.<sup>[3]</sup> After the synthesis the GO suspension was rinsed with the deionized water (pH = 5.5) multiple times by using centrifuge at 4.293,12 x g for 450 min and with a mixture of {deionized water + isopropanol} at a volume ratio 1:2 for 270 min. The supernatant was removed and the GO precipitant was dried in the oven at 100°C for several hours in air.

### *Synthesis of $\text{Fe}_3\text{O}_4$ nanoparticles*

Superparamagnetic nanoparticles were synthesized in by coprecipitation of  $\text{Fe}_3\text{O}_4$  from an aqueous solution containing  $\text{FeCl}_2$  and  $\text{FeCl}_3$  at a molar ratio 1:2 upon addition of  $\text{NH}_4\text{OH}$ .<sup>[4,5]</sup> In a vessel a mixture of 0.86 g  $\text{FeCl}_2$  and 2.35 g  $\text{FeCl}_3$  was added by 40 mL  $\text{H}_2\text{O}$  and thermally treated to 80°C under Ar via vigorous stirring. During stirring 5 mL  $\text{NH}_4\text{OH}$  was dropwise introduced into this mixture by a syringe and the heating continued for an additional 30 min. Upon slow addition of  $\text{NH}_4\text{OH}$  the solution color changed from brown to dark brown, then to black. Soon after 1 g of citric acid monohydrate in 2 mL  $\text{H}_2\text{O}$  was introduced, followed by the rise of temperature to 95°C, stirring continued for an additional 90 min. Then the reaction mixture (pH = 12) was cooled to room temperature under Ar and the black suspension was centrifuged at 8.117 x g for 30 min and the supernatant was carefully removed. The precipitant was dispersed in the deionized water (pH = 5.5) and rinsed by centrifugation three times until the final pH value of the colloidal dispersion reached 5.5. This suspension was dried in the oven at 100°C and the fine black powder was obtained. Both the suspension and obtained black powder could be easily manipulated by a force of an external static magnetic field of a permanent magnet.

### *Sonochemical synthesis of $\text{Fe}_3\text{O}_4$ -graphene oxide nanocomposites*

For the sonochemical synthesis we used a homemade horn-type ultrasonic disperser N.4-20 operating in a continuous mode at 20 kHz frequency with the 400 W maximal

output power. This ultrasonic disperser was specifically designed by Cavitation Inc. (The Republic of Belarus) for the preparation of emulsions and colloidal suspensions. The ultrasonic intensity of this device was calibrated by using a method of calorimetry.<sup>[6]</sup> Prior to the synthesis of nanocomposites 0.11 g of GO was exfoliated in 4 mL of the deionized water (pH = 5.5) by using ultrasound (8 W/cm<sup>2</sup>) for 30 min in a vessel placed in the ice bath. The exfoliated GO was triply centrifuged at 4.293,12 x g for 45 min, the supernatant was removed and the precipitant was added by aqueous solution of 44% KOH (pH = 12).

In a vessel of 40 mL H<sub>2</sub>O a mixture of {0.86 g FeCl<sub>2</sub> + 2.35 g FeCl<sub>3</sub>} was heated to 80°C under Ar under vigorous stirring for 15 min. Soon after 5 mL 44% KOH was dropwise added into this heated mixture by using a syringe and the suspension turned into a black color. This black solution was thermally treated at 80°C for an additional 30 min under Ar and a continuous stirring. Then this suspension was added by the exfoliated GO and subjected to ultrasound at 18 W/cm<sup>2</sup> for 90 min. The sonochemical synthesis was carried in a sealed reaction vessel coated by a lid connected to an Ar tube and placed in the ice bath in order to keep the temperature as low as feasible. Then the colloidal solution was triply rinsed with the deionized water at 8.117 x g for 30 min and dried at 100°C to obtain a powder. Formed nanocomposites could be easily dispersed in aqueous solution and collected by an external permanent magnet.

#### *Sonochemical functionalization of ketorolac with Fe<sub>3</sub>O<sub>4</sub>-graphene oxide nanocomposites*

Powder of Fe<sub>3</sub>O<sub>4</sub>-graphene oxide nanocomposites (30 mg) was mixed with the powder of pristine ketorolac (30 mg) and ultrasonically treated (18 W/cm<sup>2</sup>) in 11 mL of the deionized water (pH = 5.5) for 3 min under air in a vessel placed in the ice bath. Final colloidal suspension was triply rinsed with the deionized water at 8.117 x g for 15 min and dried at 100°C to obtain a powder. Formed nanocomposites could be easily dispersed in aqueous solution and collected by an external permanent magnet.

As control experiments powder of GO (30 mg) or Fe<sub>3</sub>O<sub>4</sub> nanoparticles was mixed with the powder of pristine ketorolac (30 mg) and sonicated under the same conditions followed by the thorough rinsing with the deionized water.

#### *Drug extraction test*

1 mL of each colloidal suspension containing ketorolac functionalized with Fe<sub>3</sub>O<sub>4</sub>-graphene oxide (30 mg), graphene oxide (30 mg) or Fe<sub>3</sub>O<sub>4</sub> (30 mg) nanocomposites were incubated in 1 mL of the deionized water adjusted to one of the following pH values: 1, 5 and 8. Samples were withdrawn after 7 h, rinsed by repeated centrifugation at 8.117 x g for 15 min in order to remove the unreacted chemical residuals and diluted with the deionized water for the UV-Vis absorption measurements in the use of standard rectangular quartz cuvette (volume 3.5 mL).

## Characterization

The synthesized nanocomposites, magnetite and graphene oxide were characterized through several methods: Dynamic light scattering (DLS), zeta potential (ZP), scanning electron microscopy (SEM) and energy dispersive X-ray fluorescence (EDX), X-ray powder diffraction (XRD), UV-Vis absorption and Fourier-transform infrared spectroscopies. The size distribution and  $\xi$ -potential of colloids were measured by DLS from Malvern Instruments Ltd. by using a Zetasizer Nano instrument and a buffer solution of the deionized water (pH = 5.5). DLS and  $\xi$ -potential (electrical charge) experiments were carried out on a 50 times diluted colloidal suspension. Each measurement took 10 s; the nanoparticle distribution and electrophoretic curves were obtained by averaging ten measurements.

The morphology and elemental composition of sonochemically prepared nanocomposites were analyzed by SEM (S-4800) Hitachi, Japan. The phase composition was characterized by using powder diffraction patterns recorded with an EMPYREAN diffractometer (PANalytical, Netherlands) using Cu-K $\alpha$  radiation (Ni-filter) at 296 K. The UV-Vis absorption spectra of colloidal solutions were recorded in the use of a Cary-500 spectrophotometer (Varian, USA) in the wavelength range from 200 to 800 nm. The surface chemistry and composition of nanocomposites was determined by FTIR Vertex 70 Bruker spectrometer (Germany) in the range from 400 to 4000 cm<sup>-1</sup> by using Zeiss Jena Specord-75IR (Germany).

The phase composition of GO was compared with the crystallographic data of graphite (amcsd 0000049),<sup>[7]</sup> and diamond (amcsd 0013983)<sup>[8]</sup> (Table S1).

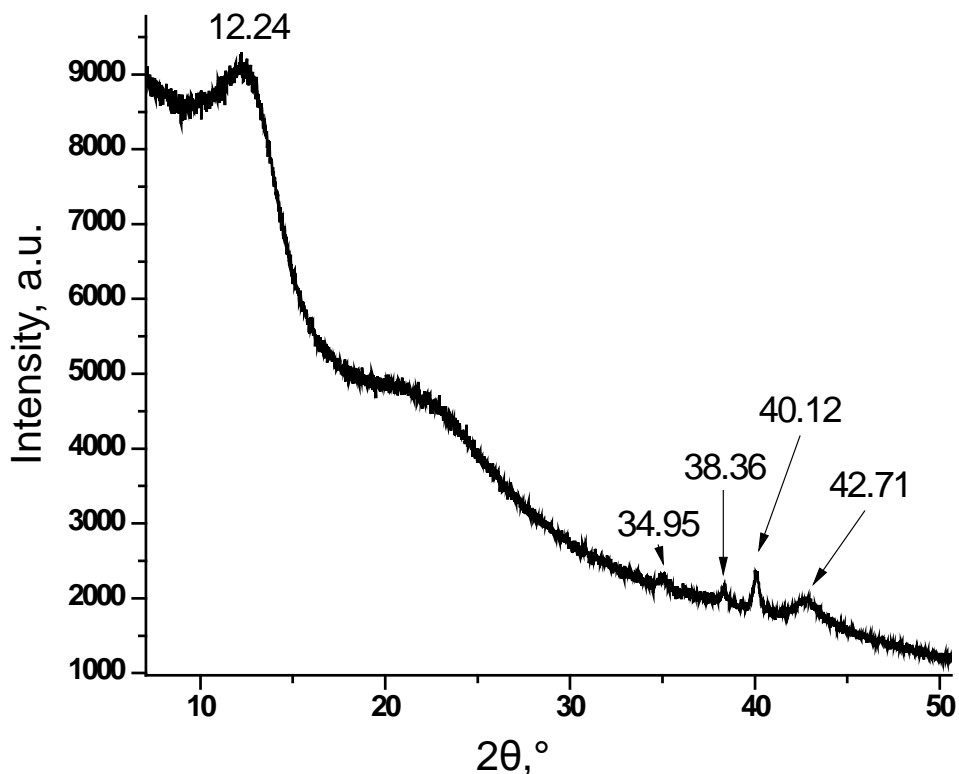


**Figure S1.** The X-Ray diffraction pattern of synthesized GO powder.

One can qualitatively estimate the state of the material according to the shape of the XRD diagram of GO. In particular, the presence of broad and low diffraction peaks demonstrates inhomogeneous material with a poor crystallinity. In contrast, narrow high peaks show homogeneous crystalline material. Most of XRD lines appear as broad and low peaks in the XRD diagram of GO. Among them the broadest line, which appears as a halo, has the angular width about  $2\theta = 10\text{-}20^\circ$  at  $\sim 22.02^\circ$  that points out to the amorphous state of GO. This amorphous state of GO may appear as a result of reflection because of the existence of the narrow order in placement of atoms in amorphous phase. This halo appears instead of a high narrow peak of (002) reflex from graphite at  $2\theta = 26.63^\circ$ .

Another broad peak at  $2\theta = 12.24^\circ$  can be related to the (001) reflex of GO being in agreement with the literature data.<sup>[9]</sup> The calculated interplanar spacing of (001) reflex is  $7.074 \text{ \AA}$  and this value is in agreement with the value of  $6.920 \text{ \AA}$  at  $2\theta = 12.70^\circ$  of GO. As the van der Waals radius of graphene is  $1.72 \text{ \AA}$ ,<sup>[10]</sup> oxygen  $1.36 \text{ \AA}$  and hydrogen  $1.17 \text{ \AA}$ , the interplanar

spacing  $d_{(001)}$  can appear due to the presence of defects in a poorly crystallized inhomogeneous graphene with the hexagonal structure consisting of four atoms of carbon and two oxygen containing groups. For comparison, the most intense X-ray line of graphite diffraction usually appears at  $2\theta = 14.95^\circ$  as a narrow high band of (001) reflex with the interplanar spacing being 6.573 Å.

On the amorphous halo of the XRD diagram one can distinguish several low peaks at  $2\theta = 34.95; 38.36; 40.12$  and  $42.71$ . The first peak can be related to the (020) reflex of diamond, which interplanar spacing agrees well with the literature. At the same time, the latest XRD peak with the calculated  $d$  value agrees very well with the (020) reflex of graphite. Neither the diffraction angle ( $38.36^\circ$ ) nor the interplanar spacing ( $2.345$  Å) of the narrow broaden peak can be related to the characteristic reflex of graphite and diamond.

On the other hand, peak at  $40.12^\circ$  can indicate rather diamond with the (021) reflex. Slightly increased value of  $d_{(021)}$  of this reflex can be caused by the influence of the amorphous phase, which contains oxygen groups, resulting in the appearance of a small peak at  $38.36^\circ$ .

**Table S1** – Experimental XRD data of diffraction angle ( $2\theta$ , °), intensity of reflex (I, a.u.), type of reflex (hkl) and calculated interplanar spacing ( $d_{hkl}$ , Å) of GO, graphite and diamond.

Experimental data of GO	$2\theta$ , °	12.24	34.95	38.36	40.12	42.71	-
	I, a.u.	28	1	1	2	1	-
	(hkl)	(001)	(020)	-	(021)	(020)	-
	$d_{hkl}$ , Å	7.07	2.56	2.35	2.27	2.12	-
Database of graphite (amcsd 0000049)	$2\theta$ , °	26.63	42.50	-	-	-	-
	I, a.u.	100	4	-	-	-	-
	(hkl)	(002)	(020)	-	-	-	-
	$d_{hkl}$ , Å	3.35	2.13	-	-	-	-
Database of diamond (amcsd 0013983)	$2\theta$ , °	20.24	32.38	34.75	40.55	41.15	41.82
	I, a.u.	2	43	100	2	20	49
	(hkl)	(001)	(111)	(020)	(021)	(002)	(201)
	$d_{hkl}$ , Å	4.39	2.77	2.58	2.23	2.19	2.16

Synthesized GO exhibits two distinct Raman bands D (disordered carbon) at  $1362\text{ cm}^{-1}$  and G (graphitic carbon) at  $1599\text{ cm}^{-1}$  with their G/D intensity ratio being about 1, suggesting GO of high quality. The appearance of a broad triple band {2D, D+G, 2G'} points out to the layered graphite structure of GO at the nanoscale.<sup>[10]</sup> The two-phonon 2D band is the second order of the D peak, which is a single peak in a monolayer graphene, i.e., this band is indicative for the stacking order of graphene sheets along the *c* axis. This 2D mode at  $2730\text{ cm}^{-1}$  is observed at higher wavenumbers (at  $\sim 50\text{ cm}^{-1}$ ) than in a single-layer graphene ( $\sim 2680\text{ cm}^{-1}$ ) because of the lower concentration of electrons, i.e. due to the hole doping effect.<sup>[11]</sup> The {D+G} band can arise due to the combination of phonons with the different momenta, and indicates nanocrystalline disordered clusters, in agreement with our observation of the D band. In this triple band the 2G' peak is a second order of the D' band (characteristic peak at  $1620\text{ cm}^{-1}$ , indicating the structural disorder and the presence of small grains,<sup>[12]</sup> and usually appears in defective samples. This band appears with a negligibly small intensity and can be hardly distinguished in a triple second-order band, demonstrating that only some very small defects can be developed in the GO structure.

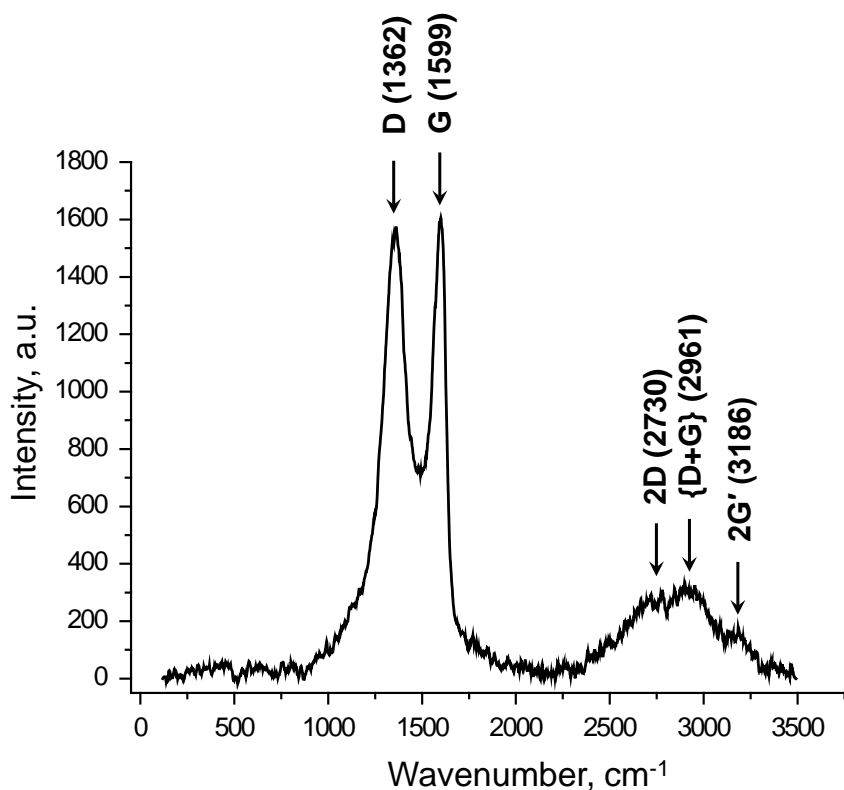


**Figure S2.** Raman spectrum of synthesized GO powder (the laser excitation wavelength is 473 nm and the incident power is 5 mW).

The elemental composition of synthesized GO is shown in the Energy Dispersive X-Ray spectrum. There are two most prominent peaks in this EDX spectrum: one is assigned to carbon (C, at. 64.28 %) and another – to oxygen (O, at. 35.17 %), more details can be found in Table S2. The concentration of impurities in GO is negligible.

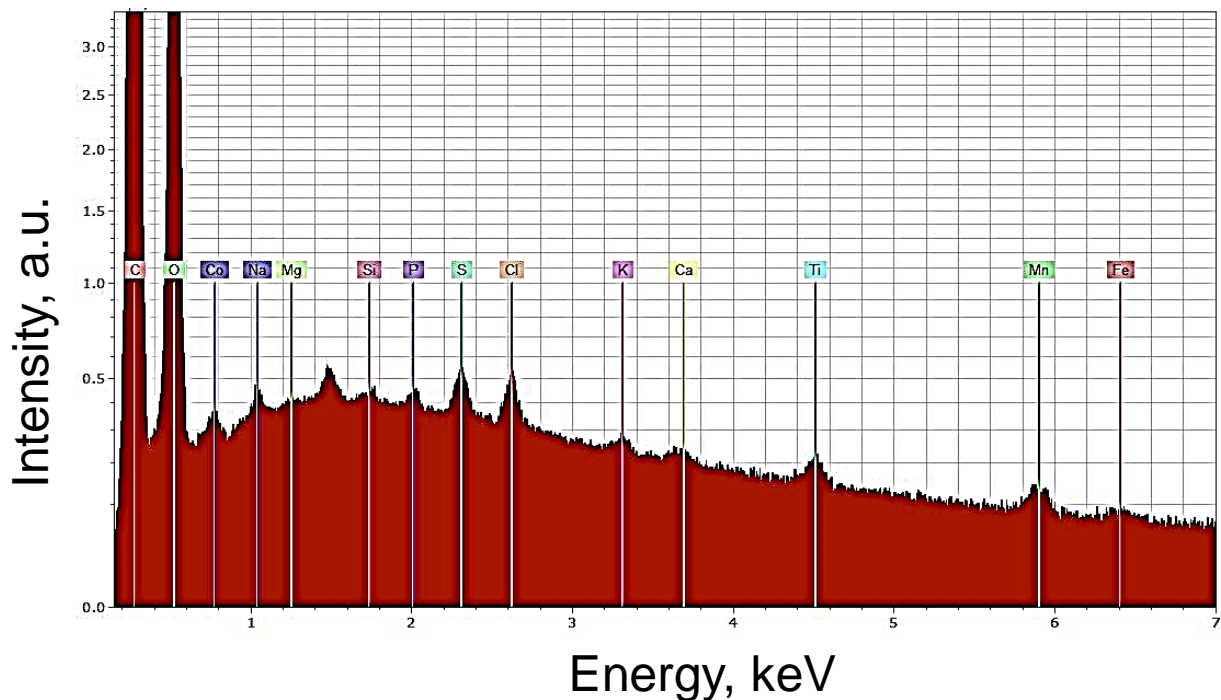


**Figure S3.** Energy Dispersive X-Ray spectrum of synthesized GO after interaction with the incident flow of electrons under 14.8 kV.

**Table S2.** Experimental data from the EDX spectrum of synthesized GO.

Element	Atomic number	Atom. C, at. %	Error, wt. %
Carbon (C)	6	64.28	6.0
Oxygen (O)	8	35.17	4.5
Chlorine (Cl)	17	0.09	0.0
Sulfur (S)	16	0.09	0.0
Sodium (Na)	11	0.08	0.0
Manganese (Mn)	25	0.08	0.0
Titanium (Ti)	22	0.06	0.0
Potassium (K)	19	0.03	0.0
Iron (Fe)	26	0.03	0.0
Calcium (Ca)	20	0.03	0.0
Phosphorus (P)	15	0.02	0.0
Silicon (Si)	14	0.02	0.0

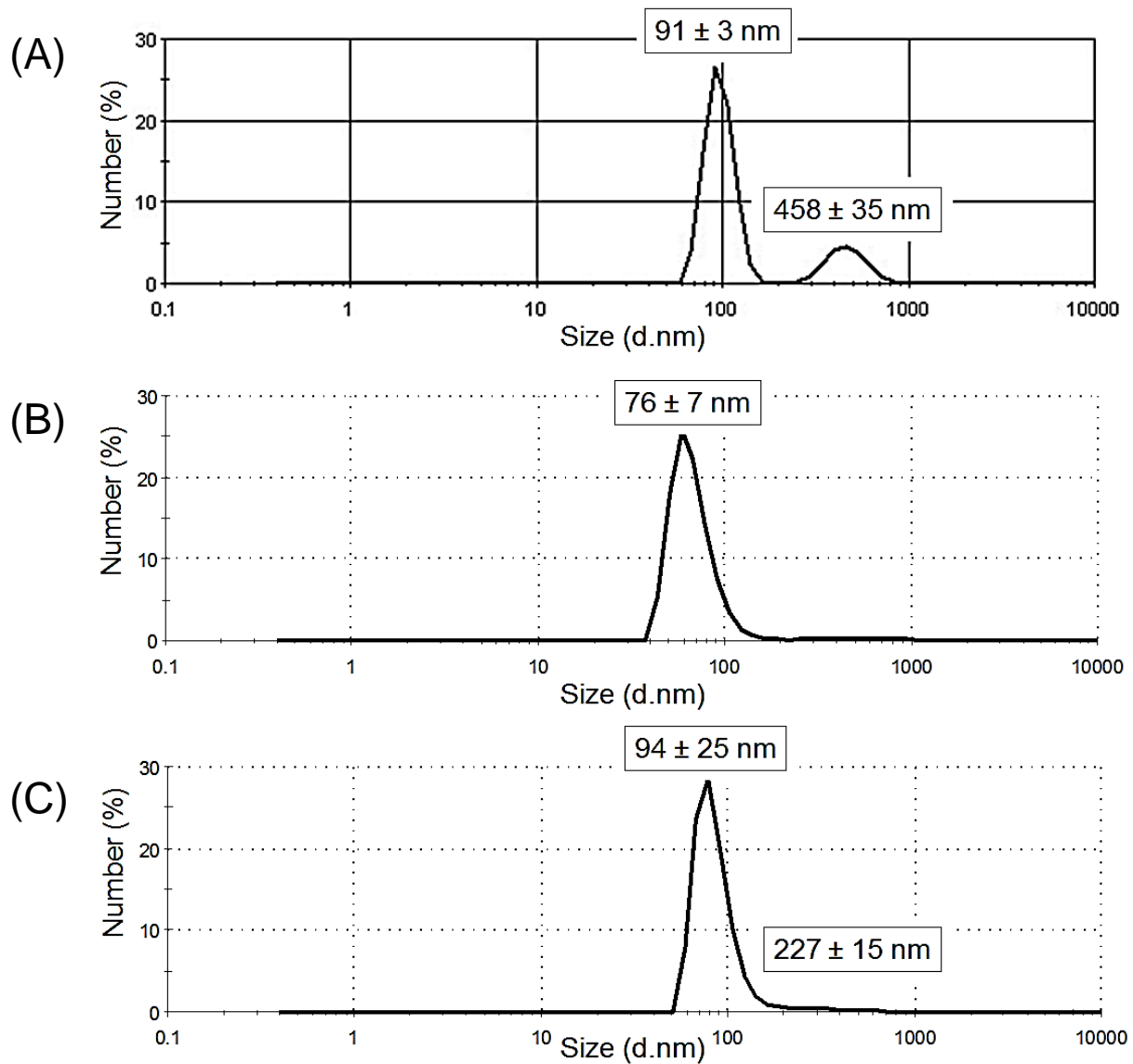


**Figure S4.** Dynamic light scattering diagrams of (A) synthesized GO, (B) preformed magnetite nanoparticles and (C) sonochemically prepared  $\text{Fe}_3\text{O}_4$ -GO nanocomposite.

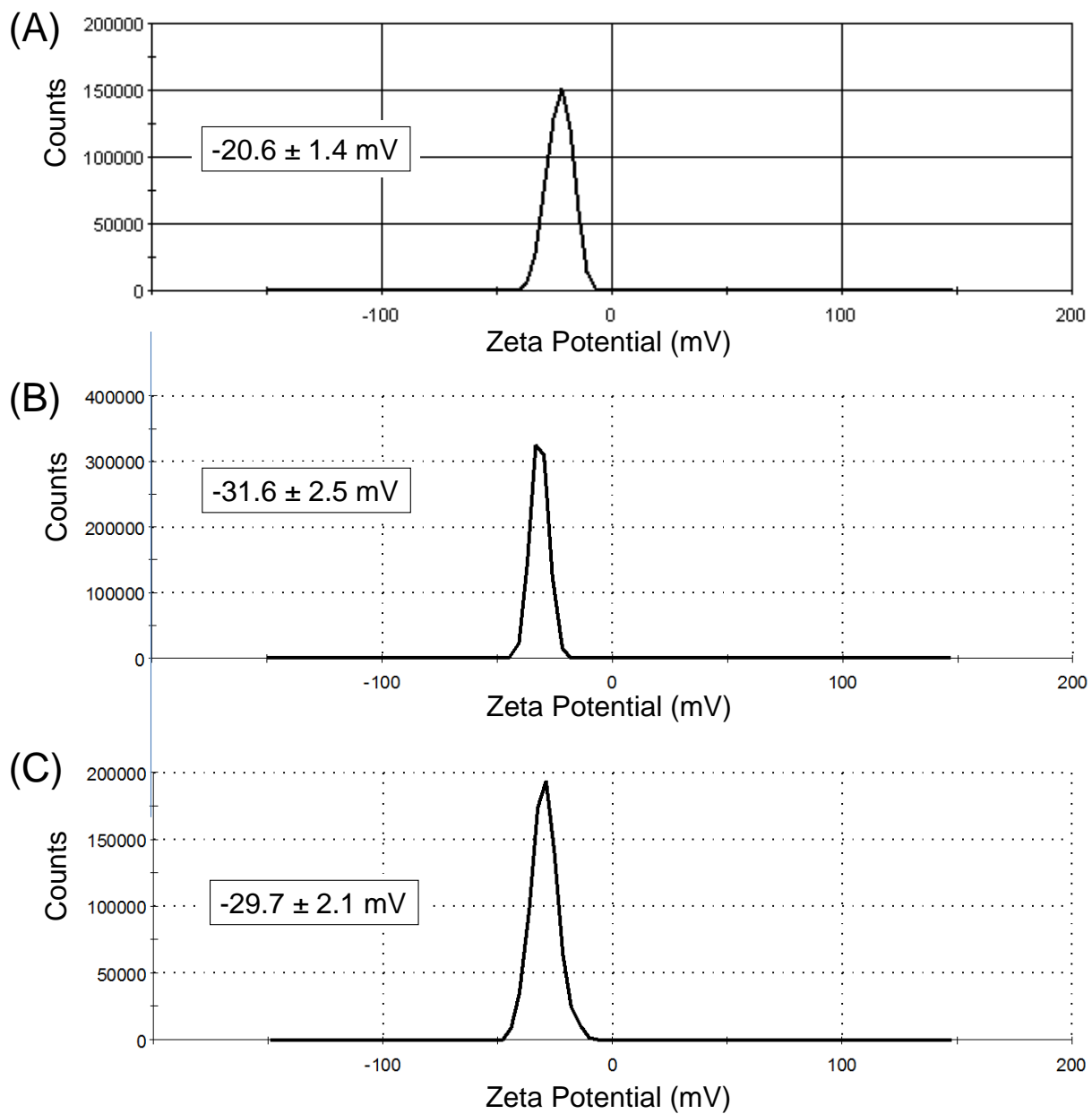


**Figure S5.** Zeta potential diagrams of (A) synthesized GO, (B) preformed magnetite nanoparticles and (C) sonochemically prepared  $\text{Fe}_3\text{O}_4$ -GO nanocomposite.

**Table S3.** The measured X-Ray powder diffraction values of diffraction angle ( $2\theta$ , °), intensity of reflex (I, a.u.) and the calculated interplanar spacing ( $d_{hkl}$ , Å) of the sonochemically synthesized Fe<sub>3</sub>O<sub>4</sub>-GO nanocomposite in comparison to the database of magnetite (amcsd 0013895), graphite (amcsd 0000049) and diamond (amcsd 0013983).

Synthesized Fe <sub>3</sub> O <sub>4</sub> -GO				Fe <sub>3</sub> O <sub>4</sub> (amcsd 0013895)			
2θ, °	I, a.u.	(hkl)	$d_{hkl}$ , Å	2θ, °	I, a.u.	(hkl)	$d_{hkl}$ , Å
12.52	46	(001)	7.31	-	-	-	-
18.21	46	(111)	4.87	18.28	7	(111)	4.85
21.33	52	(001)	4.09	-	-	-	-
27.02	42	(002)	3.34	-	-	-	-
30.17	47	(220)	2.96	30.07	28	(220)	2.97
31.98	33	(111)	2.78	-	-	-	-
34.61	48	(020)	2.60	-	-	-	-
35.47	100	(311)	2.53	35.42	100	(311)	2.53
37.87	23	(222)	2.37	37.05	8	(222)	2.42
40.85	15	(021)	2.22	-	-	-	-
43.28	27	(400)	2.09	43.05	20	(400)	2.10
53.40	17	(422)	1.72	53.41	9	(422)	1.72
57.25	26	(511)	1.61	56.93	24	(511)	1.62
62.94	39	(220)	1.48	62.52	6	(220)	1.49
70.18	10	(311)	1.34	70.92	40	(311)	1.33
74.03	12	(222)	1.28	73.95	8	(222)	1.28
75.19	9	(400)	1.26	74.95	3	(400)	1.27

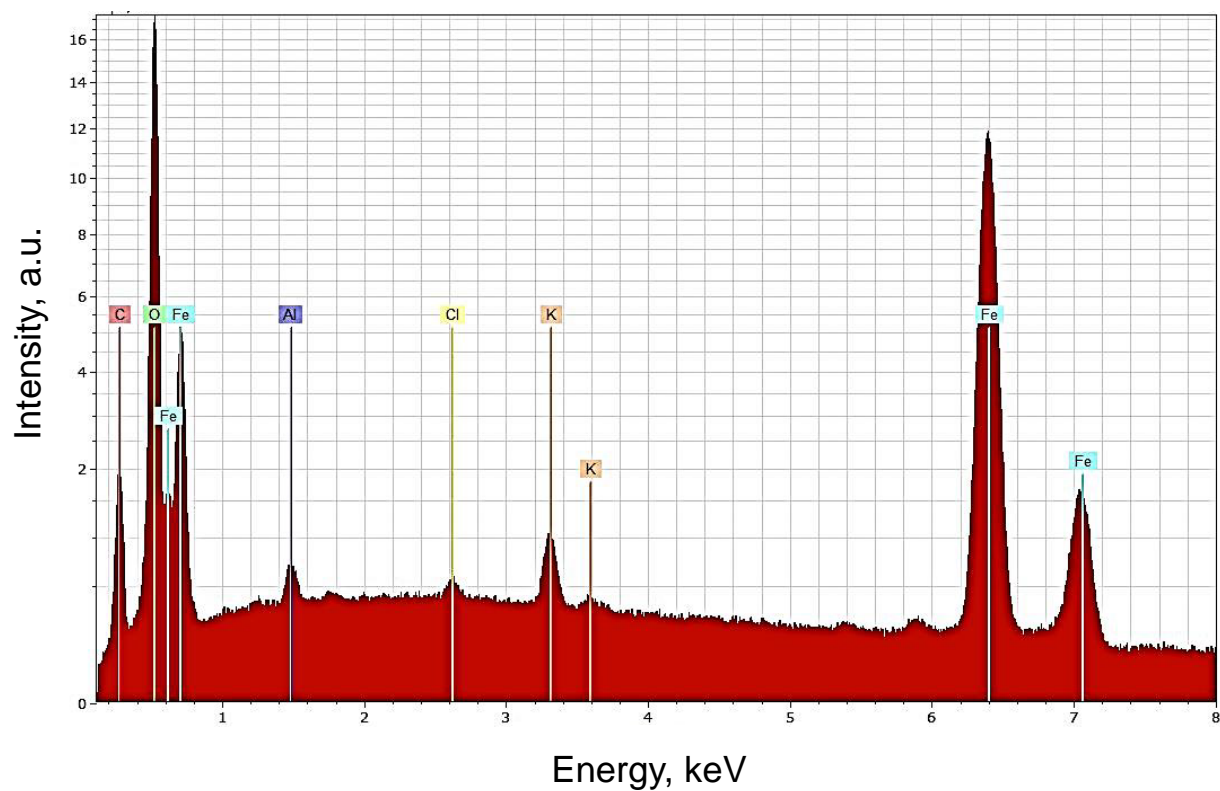


**Figure S6.** The Energy Dispersive X-Ray spectrum of sonochemically formed  $\text{Fe}_3\text{O}_4$ -GO nanocomposite after interaction with the incident flow of electrons under 20.0 kV.

**Table S4.** The elemental composition of sonochemically prepared Fe<sub>3</sub>O<sub>4</sub>-GO nanocomposite obtained from the EDX spectra.

<b>Element</b>	<b>Atomic number</b>	<b>Atom.C [at. %]</b>	<b>Error [wt. %]</b>
Oxygen (O)	8	59.62	4.8
Iron (Fe)	26	22.94	1.6
Carbon (C)	6	16.36	1.2
Potassium (K)	19	0.59	0.1
Aluminium (Al)	13	0.38	0.0
Chlorine (Cl)	17	0.12	0.0

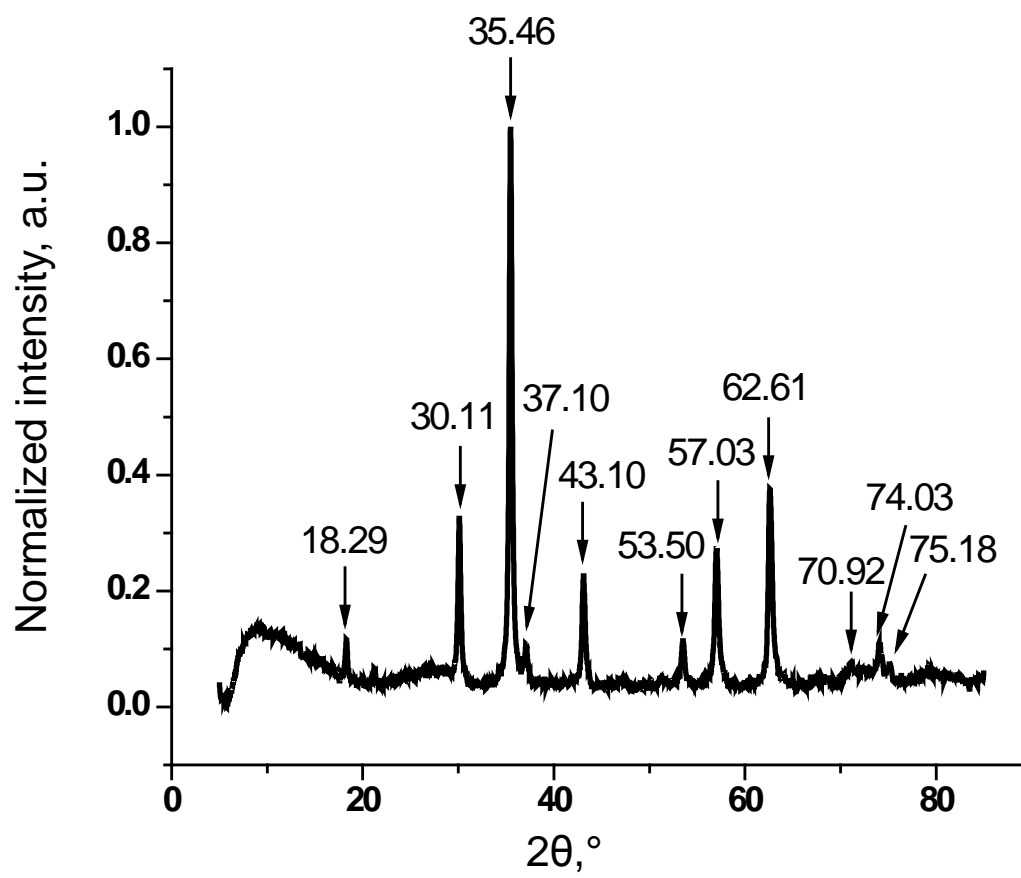


**Figure S7.** X-Ray powder diffraction pattern of synthesized Fe<sub>3</sub>O<sub>4</sub> nanoparticles.

**Table S5.** The measured X-Ray powder diffraction values of diffraction angle ( $2\theta$ , °), intensity of reflex (I, a.u.) and the calculated interplanar spacing ( $d_{hkl}$ , Å) of synthesized  $\text{Fe}_3\text{O}_4$  nanoparticles.

<b>Synthesized <math>\text{Fe}_3\text{O}_4</math> nanoparticles</b>			
<b><math>2\theta</math>, °</b>	<b>I, a.u.</b>	<b>(hkl)</b>	<b><math>d_{hkl}</math>, Å</b>
18.29	8	(111)	4.85
30.11	29	(220)	2.97
35.46	96	(311)	2.53
37.10	7	(222)	2.42
43.10	19	(400)	2.10
53.50	8	(422)	1.72
57.03	24	(511)	1.62
62.61	35	(220)	1.48
70.92	4	(311)	1.33
74.03	7	(222)	1.28
75.18	3	(400)	1.27

The FTIR spectrum of the synthesized GO reveals the presence of sulfur ions as indicated by the vibration of P-S/P=S groups at  $503\text{ cm}^{-1}$  and  $555\text{ cm}^{-1}$ , C-S groups at  $625\text{ cm}^{-1}$  and  $\text{SO}_4^{2-}$  at  $638\text{ cm}^{-1}$ . The S-S modes (vibration near  $600\text{ cm}^{-1}$ ) are also present as a result of intercalation of sulfur atoms into the GO structure. In this spectrum a weak band is located at  $1087\text{ cm}^{-1}$  pointing out to the  $\nu(\text{C}=\text{O})$  vibration. Two strong bands appear at  $1153\text{ cm}^{-1}$  and  $1230\text{ cm}^{-1}$  as a result of the CO bonds in epoxy (-C-O-C-) groups and at  $1400\text{ cm}^{-1}$  of the C-C carbon network. The presence of carboxyl groups on the GO surface is confirmed by the stretching mode of the carbonyl group  $\nu(\text{C}=\text{O})$  at  $1726\text{ cm}^{-1}$ . The OH deformation in dimers of carboxylic groups ( $\sim 1621\text{ cm}^{-1}$ ) indicates that the initially conjugated  $\pi$ -orbital system of the natural graphite was damaged by the insertion of CO groups into the carbon skeleton.<sup>[14]</sup>

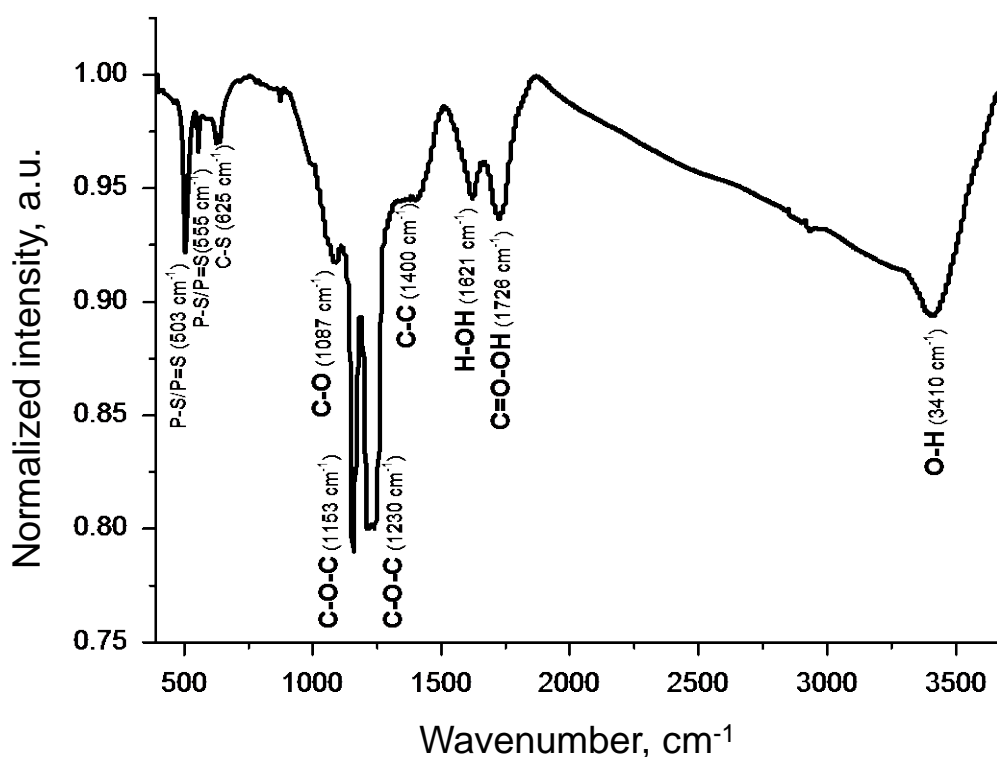


**Figure S8.** Fourier transform infrared (FTIR) transmittance spectrum of synthesized GO.

In the UV-Vis absorption, there are no transitions in pristine ketorolac involving the  $\sigma$  (bonding) molecular orbital (-C-C-) that is commonly assigned to the covalent bonding between carbon atoms within a plane. We assume that relatively weak van der Waals forces control the molecular interactions of ketorolac involving the bonding ( $\pi$  orbitals) and anti-bonding ( $\pi^*$  orbitals) in the valence and conduction bands. The appearance of two types of transitions:  $^1(\pi_{py} \rightarrow \pi^*_{CO})$  at 246 nm and  $^1(n_O \rightarrow \pi^*_{CO})$  at 322 nm demonstrates that ketorolac molecules have unsaturated centers and require less energy for their electronic excitation than transitions to  $\sigma^*$  antibonding orbitals. Both transitions in ketorolac are characterized by the anti-bonding  $\pi^*$  orbital of the  $C_3O_1$  moiety, indicating that this type of molecular orbital weakens the chemical bond between two atoms and avails to raise the energy of the molecule relative to the separated atoms. On the other hand, the anti-bonding  $\pi^*$  orbital may inhibit bonding (i.e. interaction between several atoms or their groups that hold the atoms together) because both electrons are present in an orbital, in contrast to the bonding, where an orbital is occupied by a single electron instead of two.

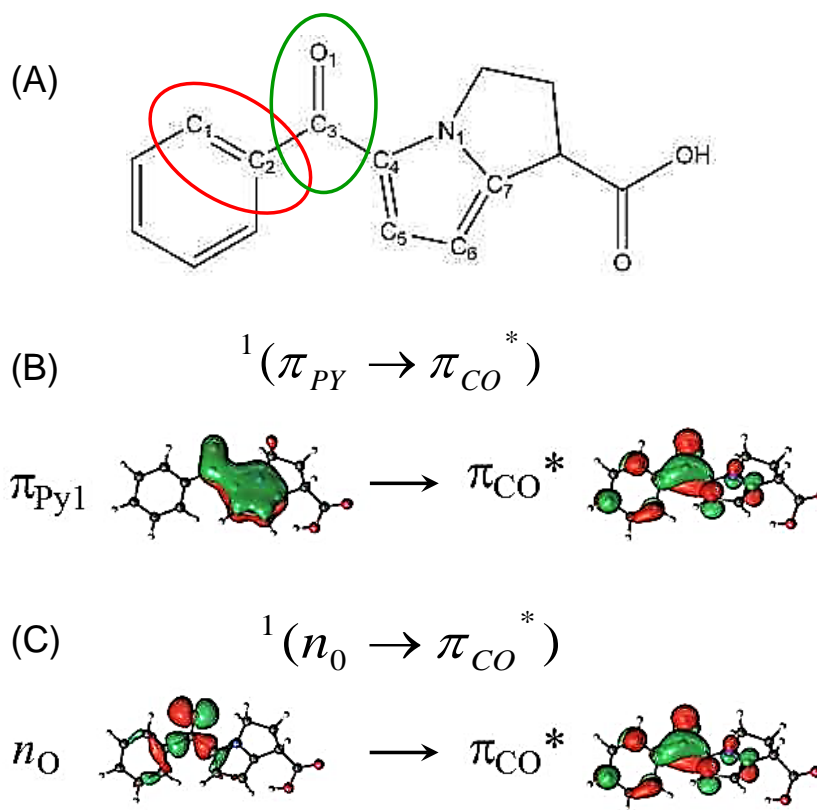


**Figure S9.** (A) The chemical structure of ketorolac with the labelled and numbered atoms. (B) and (C) Computed molecular orbitals of ketorolac in the use of DFT and CASSCF/CASPT2 methods as implemented in the Gaussian 09 and MOLCAS 7.6 quantum-chemical packages of software,<sup>[15]</sup> adapted from the reference.<sup>[16]</sup>

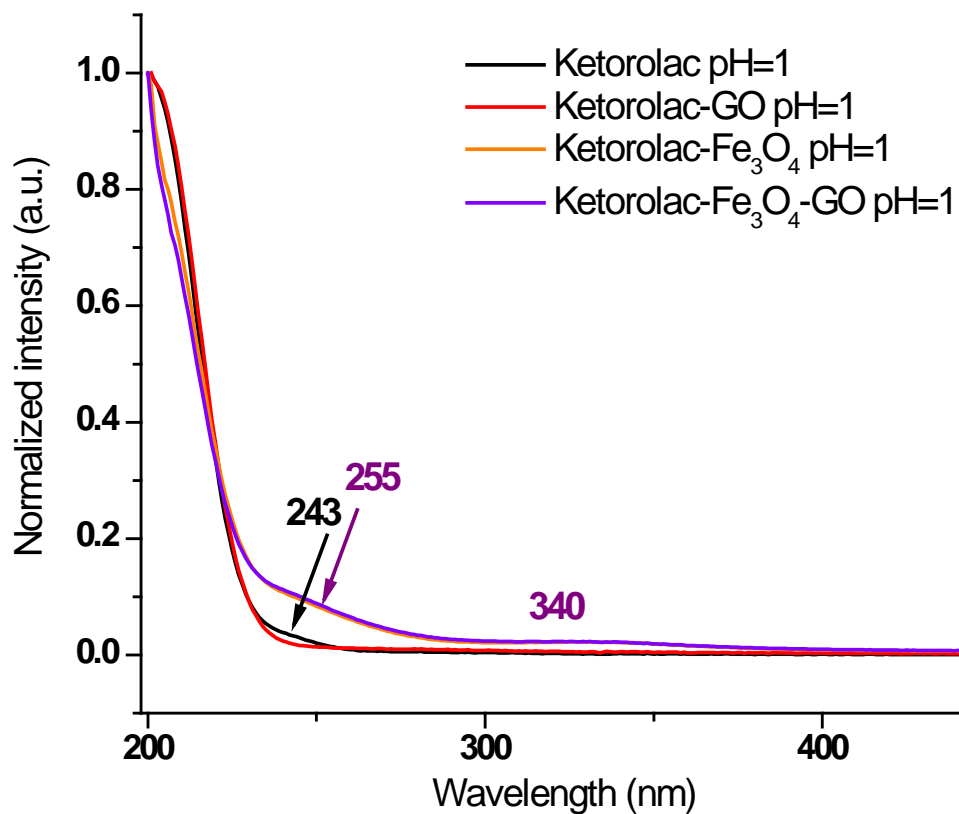


**Figure S10.** UV-Vis absorption spectra of pristine ketorolac and its nanocomposites: ketorolac- $\text{Fe}_3\text{O}_4$ , ketorolac-GO in comparison to the ketorolac-  $\text{Fe}_3\text{O}_4$ @GO material after 7 h of incubation in highly acidic solution of the deionized water (pH = 1) and triple rinses by centrifugation at 8.117 x g for 30 min.

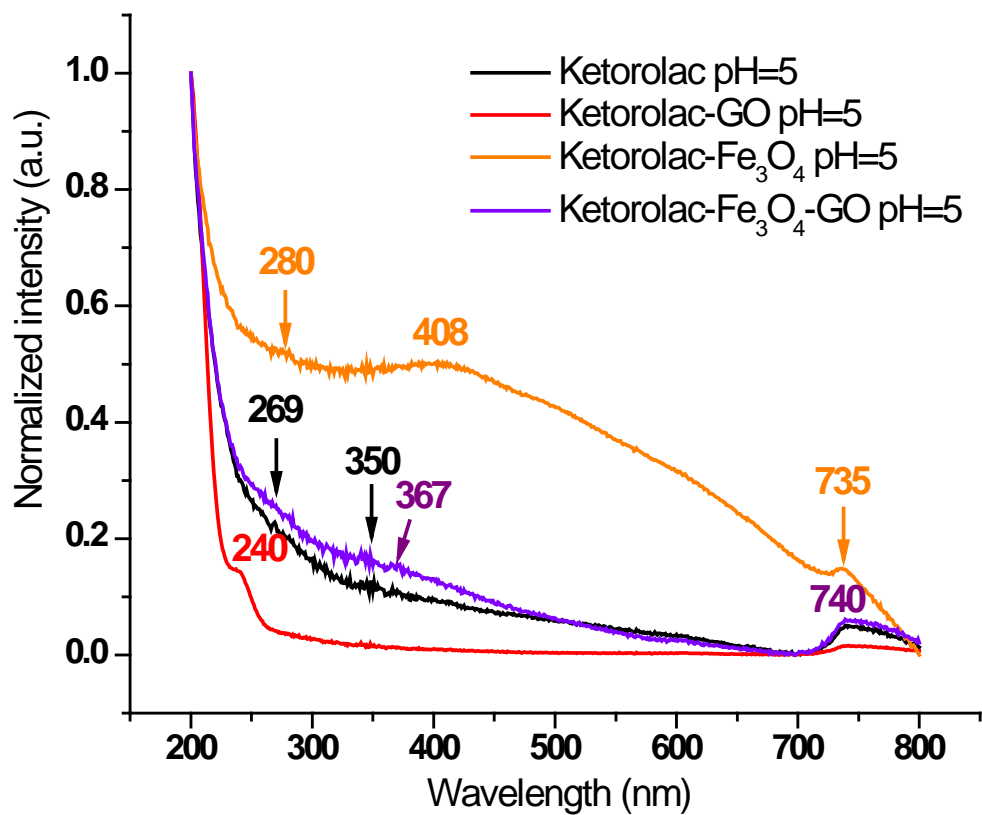


**Figure S11.** UV-Vis absorption spectra of pristine ketorolac and its nanocomposites: ketorolac-Fe<sub>3</sub>O<sub>4</sub>, ketorolac-GO in comparison to the ketorolac-Fe<sub>3</sub>O<sub>4</sub>@GO material after 7 h of incubation in the deionized water (pH = 5) and triple rinses by centrifugation at 8.117 x g for 30 min.

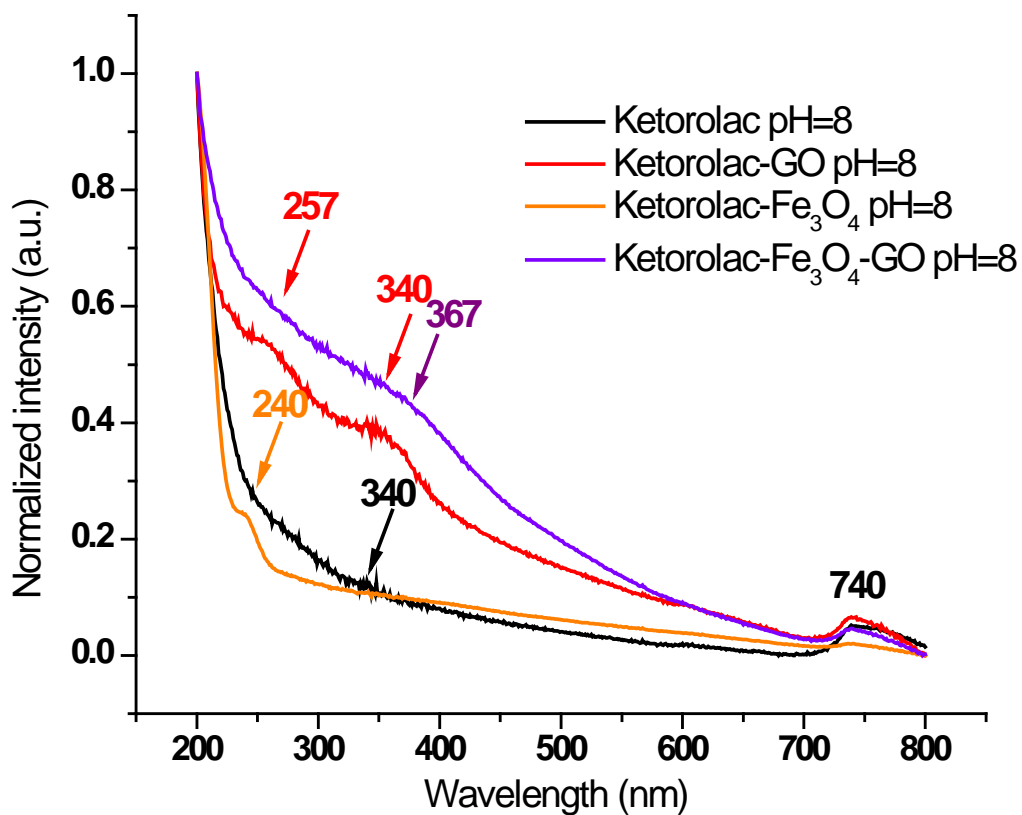


**Figure S12.** UV-Vis absorption spectra of pristine ketorolac and its nanocomposites: ketorolac-Fe<sub>3</sub>O<sub>4</sub>, ketorolac-GO in comparison to the ketorolac-Fe<sub>3</sub>O<sub>4</sub>@GO material after 7 h of incubation in the deionized water (pH = 8) and triple rinses by centrifugation at 8.117 x g for 30 min.

## References

- [1] D. Radziuk, L. Mikhnavets, V. Mykhailo, V. Matolín, L. Tabulina and V. Labunov, *Chem. Eur. J* **2019**, *25*, 6233–6245.
- [2] D. C. Marcano, D. V. Kosynkin, J. M. Berlin, A. Sinitskii, Z. Sun, A. Slesarev, L. B. Alemany, W. Lu and J. M. Tour, *ACS Nano* **2010**, *4*, 4806–4814.
- [3] D. Radziuk, L. Mikhnavets, A. Tkach, L. Tabulina and V. Labunov, *Langmuir* **2018**, *34*, 8599–8610.
- [4] R. Massart, *IEEE Transactions on Magnetics* **1981**, *17*, 1247–1248.
- [5] Y. Sahoo, A. Goodarzi, M. T. Swihart, T. Y. Ohulchanskyy, N. Kaur, E. P. Furlani and P. N. Prasad, *J. Phys. Chem. B* **2005**, *109*, 3879–3885.
- [6] M. A. Margulis and I. M. Margulis, *Ultrasonics Sonochemistry* **2003**, *10*, 343–345.
- [7] J. S. Kukulski, L. Pauling, *Am. Mineral.* **1950**, *35*, 125.
- [8] J. Fayos, *J. Solid State Chem.* **1999**, *148*, 278–285.
- [9] H. C. Schniepp, J.-L. Li, M. J. McAllister, H. Sai, M. Herrera-Alonso, D. H. Adamson, R. K. Prud'homme, R. Car, D. A. Saville, I. A. Aksay, *J. Phys. Chem. B* **2006**, *110*, 8535–8539.
- [10] K. S. Novoselov, A. K. Geim, S. V. Morozov, D. Jiang, Y. Zhang, S. V. Dubonos, I. V. Grigorieva, A. A. Firsov, *Science* **2004**, *306*, 666–669.
- [11] E. H. M. Ferreira, M. V. O. Moutinho, F. Stavale, M. M. Lucchese, R. B. Capaz, C. A. Achete, A. Jorio, *Phys. Rev. B* **2010**, *82*, 125429.
- [12] A. Das, S. Pisana, B. Chakraborty, S. Piscanec, S. K. Saha, U. V. Waghmare, K. S. Novoselov, H. R. Krishnamurthy, A. K. Geim, A. C. Ferrari, A. K. Sood, *Nat. Nanotechnol.* **2008**, *3*, 210–215.
- [13] L. G. Cançado, A. Jorio, E. H. M. Ferreira, F. Stavale, C. A. Achete, R. B. Capaz, M. V. O. Moutinho, A. Lombardo, T. S. Kulmala, A. C. Ferrari, *Nano Lett.* **2011**, *11*, 3190–3196.
- [14] M. Sametband, U. Shimanovich, A. Gedanken, *New J. Chem.* **2012**, *36*, 36–39.
- [15] F. Aquilante, L. De Vico, N. Ferré, G. Ghigo, P.-Å. Malmqvist, P. Neogrady, T. B. Pedersen, M. Pitoňák, M. Reiher, B. O. Roos, L. Serrano-Andrés, M. Urban, V. Veryazov, R. J. Lindh, *J. Comput. Chem.* **2010**, *31*, 224–227.
- [16] C. D. McTiernan, C. Fasciani, M. González-Béjar, D. Roca-Sanjuán, E. I. Alarcon, J. C. Netto-Ferreira, *MedChemComm* **2013**, *4*, 1619–1622.